ACS OMEGA

http://pubs.acs.org/journal/acsodf

Article

Size, Shape, and Phase of Nanoscale Uric Acid Particles

Dewansh Rastogi and Akua Asa-Awuku*

Cite This: *ACS Omega* 2022, 7, 24202−24207

Read Online

ACCESS | Metrics & More | Article Recommendations | Supporting Information

ABSTRACT: Uric acid particles are formed due to hyperuricemia, and previous works have focused on understanding the surface forces, crystallization, and growth of micron- and supermicron-sized particles. However, little to no work has furthered our understanding about uric acid nanonuclei that precipitate during the initial stages of kidney stone formation. In this work, we generate nanosized uric acid particles by evaporating saturated solution droplets of uric acid. Furthermore, we quantify the effects of drying rate on the morphology of uric acid nanonuclei. An aerosol droplet drying method generates uric acid nanoparticles in the size range of 20−200 nm from aqueous droplets (1−6 μm). Results show that uric acid nanonuclei are non-spherical with a shape factor value in the range of 1.1−1.4. The shape factor values change with drying rate and indicate that the nanoparticle morphology is greatly affected by drying kinetics. The nanonuclei are amorphous but can grow to form crystalline micron-sized particles. Indeed, a pre-crystallization phase was observed for heterogeneous nucleation of uric acid particles in the size range of a few hundred nanometers. Our findings show that the morphology of uric acid nanonuclei is significantly different from that of crystalline supermicron-sized particles. These new findings imply that the dissolution characteristics, surface properties, elimination, and medical treatment of uric acid nanonuclei formed during the initial stages of nucleation must be reconsidered.

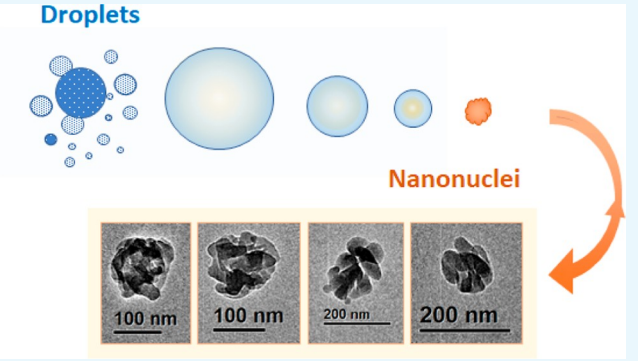

1. INTRODUCTION

The prevalence of kidney stone cases is increasing globally. Specifically, 1 in every 11 persons in the United States is likely to report having kidney stones in their lifetime.[1] An individual's risk of kidney stone formation has been linked to genetics, lifestyle, environmental changes, and personal dietary choices,[1,2] and thus, understanding the chemical and physical processes that result in the precipitation of stones is of scientific interest.

The kidney stone formation process can be divided into three steps: nucleation, growth, and aggregation.[3,4] During the heterogeneous nucleation process, small uric acid nuclei (on the nanoscale) precipitate from the surrounding saturated aqueous solution in the presence of salts. These nuclei grow and aggregate over time to form stones, causing discomfort, inflammation, and pain. It should also be noted that the real-world process of stone formation in vivo is heterogeneous; differences in mucosal material, urinary pH, and the ionic strength of dissolved impurities are examples of the complexities that challenge experimental replication under controlled laboratory conditions. The current medical treatment uses shockwaves, followed by chemodissolution to remove the crystalline deposits.[5,6] In extreme occurrences, when the kidney stone is too big to be broken down safely, surgery is considered as the last resort.

Early publications observed uric acid crystals formed from the saturated solution phase; crystals in size ranges of a few millimeters were described as winged, platy, and dendritic.[6,7] Chemical force microscopy (CFM) and atomic force microscopy (AFM) experimental techniques have measured in situ growth rates and forces acting on the surfaces of uric acid crystals. CFM and AFM work indicated that the dominant forces of attraction between crystals depended on the surrounding solution and were likely to be van der Waals and electrostatic interactions.[8−10] Thus, the particle growth via aggregation of uric acid crystals has been well characterized. It is important to note that the aforementioned studies have been conducted in supermicron sizes; little to no work has been done to understand the formation of nanonuclei that act as seeds toward the formation of larger kidney stones. Nanonuclei are explicitly challenging to study because of their inherently small size and the fast rate of formation.

Droplet drying and evaporation can be used to study the precipitation of solute from the solution phase. As a droplet

Received: February 28, 2022
Accepted: June 13, 2022
Published: July 5, 2022

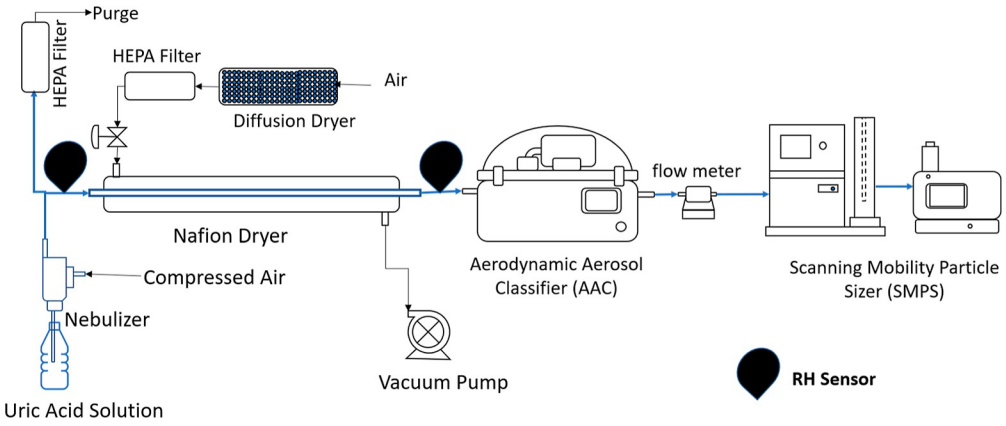

Figure 1. Experimental setup to measure the aerodynamic diameter (d_{ae}) and electrical mobility diameter (d_{mo}) of uric acid. Measured sizes are used to calculate the particle shape factor, χ.

dries, the concentration of the solute increases in the solution phase eventually reaching saturation and causing solute precipitation. The method of droplet drying is also useful to study the formation of nanoparticles as it arrests the growth of particles at the initial stages of formation, and these nanoparticles can then be probed to study their physical properties. In this work, we use well-established droplet drying methods[11,12] to study the formation of uric acid nanoparticles, which has not been studied before. The generation of wet droplets is a standard practice in industries that create powders with specified aerosol physical properties (e.g., but not limited to food science, pharmaceuticals, and cosmetics). The physical properties of the powders are controlled by the concentration, flow rates, and drying rates.[13−15] In this work, aqueous droplets of uric acid are generated with an aerosol nebulizer. The wet particles are then dried under controlled experimental conditions and then characterized using aerodynamic and electrical mobility forces to study the morphological (size, shape, and structure) changes in the dried nanoparticles. To our knowledge, the formation and characterization of nanoscale uric acid particles has not been shown before. Specifically, we show evidence of amorphous uric acid particle formation less than 1 μm in size and use microscopic techniques to show images of the shape and morphology of uric acid nanonuclei. Furthermore, we measure the in situ particle size and define the effects of drying rate on particle shape. Understanding the precipitation processes that govern nanoscale particle formation and subsequent aggregation to micron sizes will improve our understanding of kidney stone formation and dissolution in the body.

2. EXPERIMENTAL METHODS

Uric acid particles were generated with two techniques. The first method generates particles by drying the aqueous solution onto a carbon tape. The second technique uses a droplet drying method to form in situ aerosol. Specifically, an aqueous solution (0.1 gL^{-1}) of uric acid (Sigma-Aldrich, 99% crystalline) in ultra-purified water (Millipore, <18 mΩ) was prepared to generate in situ aerosol particles. The solution was aerosolized with a commercial nebulizer (TSI 3076) using compressed filtered air at 15 psig (Figure 1). The nebulized aqueous uric acid droplets were then dried using a Nafion dryer (Perma Pure, MD-700). The drying rate was regulated by varying the vacuum strength on the shell side of the Nafion dryer using a needle valve and a vacuum pump. The vacuum on the shell side varied between −5 and −20 mm Hg. Nanoscale-dried particles were then sampled for imaging or measured in real time for their physical particle properties. In situ dried particles were also selected by their aerosol size. Specifically, the dried aerosol stream was passed through an aerodynamic aerosol classifier (AAC, Cambustion). The AAC selects the particle aerodynamic diameter (d_{ae}), and it has been described in detail by the following papers.[16−19]. In this experiment, particles with an aerodynamic diameter from 90 to 200 nm were size-selected. Ten discrete sizes were chosen, and each monodispersed aerodynamic diameter size was subsequently measured by a scanning mobility particle sizer (SMPS, Electrostatic Classifier model 3082 and Condensation Particle Counter 3776, TSI) to obtain the corresponding mobility diameter (d_{mo}). Each SMPS scan took 2.15 min and was repeated three times for each d_{ae}. Measurements were performed at 0.3 L min^{-1}, and the sample-to-sheath flow ratio for SMPS and AAC was maintained at 1−10. The working principles of SMPS and AAC have been discussed extensively by Wang and Flagan (1989) and Tavakoli and Olfert (2013). The tandem SMPS and AAC measurement allows for independent determination of the mobility and aerodynamic diameters and results in measurement with <10% uncertainty.[18] The relative humidity (RH) and temperature were measured for the aerosol stream at the inlet and exit of the drying tube and were maintained above 70% and below 20%, respectively. The ambient RH and temperature were monitored to ensure the repeatability of measurements.

The in situ particle shape can be quantified with a shape factor, χ, parameter. The shape factor is the ratio of forces acting on a non-spherical particle to forces on a volume equivalent sphere.[20]

$$\chi = \frac{F_D^p}{F_D^{Ve}} \quad (1)$$

Here, F_D^p is the drag force acting on the particle and F_D^{Ve} is the drag force acting on a volume equivalent sphere. The drag forces applied in tandem AAC and SMPS measurements can be directly compared, and the shape factor can be derived from the measurements of d_{ae} and d_{mo} (see the Supporting Information).

Two imaging techniques were applied to visualize the uric acid particles. Transmission electron microscopy (TEM) was used for nanoscale aerosol, and scanning electron microscopy (SEM) was applied to micron-scale particles. Micron-sized

https://doi.org/10.1021/acsomega.2c01213
ACS Omega 2022, 7, 24202−24207

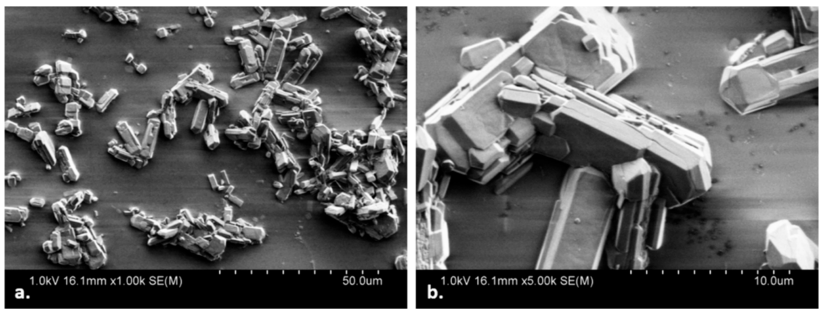

Figure 2. SEM images of uric acid crystallized from aqueous solution dried on carbon tape. Images at (a) 1000× magnification and (b) 5000× magnification.

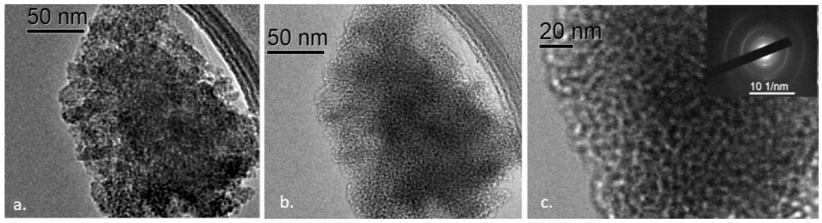

Figure 3. (a) TEM image of uric acid droplet dried on a Lacey carbon copper TEM grid. (b,c) show HRTEM images—pre-crystallization zones in amorphous nanonuclei. The inset image in (c) shows the particle diffraction pattern indicating an amorphous phase.

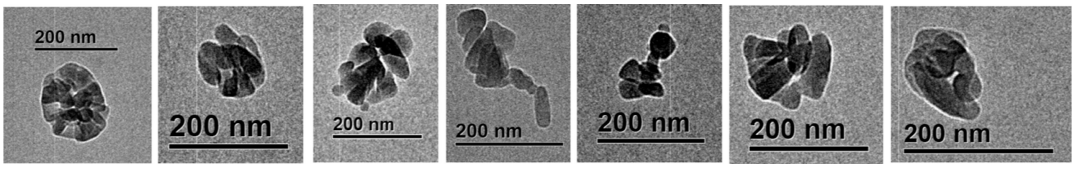

Figure 4. Image shows aerosol particles quickly dried at a vacuum pressure of −20 mm Hg in the shell side of the Nafion dryer.

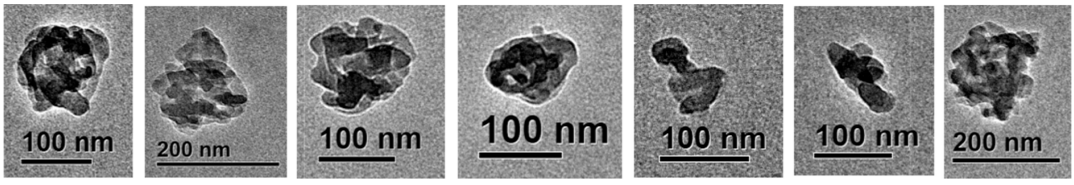

Figure 5. Image shows uric acid aerosol dried at a vacuum pressure of −5 mm Hg in the shell side of the Nafion dryer.

particles for SEM were generated by drying aqueous uric acid droplets onto carbon tape at 7 ± 2% RH and 22 ± 3 °C. To ensure particle growth to the micron size range, the process of evaporation was carried out four times with saturated uric acid solution. The crystallized uric acid particles were then imaged using a Hitachi SU-70 SEM at a magnification of 1000× to 5000×. The uric acid particles are non-conductive, and thus, additional processing of the sample (e.g., gold coating) would be required to visualize the nano-sized particles with SEM techniques.

Particles less than 400 nm were charged (Kr-85 neutralizer, TSI) and deposited on an electrically grounded, lacey carbon-coated copper TEM grid (TED PELLA, 400 mesh CU). The process was performed for drying pressures of −5 mm Hg and −20 mm Hg. Each sample was collected for 6 h to ensure sufficient particle concentration on the TEM grids. High-resolution TEM (HRTEM) and selected area electron diffraction (SAED) pattern analyses provided information about the existence of repeating structures, such as unit cells in lattice structures, used to infer the phase of submicron particles.

3. RESULTS AND DISCUSSION

SEM analysis shows crystallized uric acid particles in the size range of 1−20 μm (Figure 2). Again, SEM-imaged particles are not in situ and were generated by drying saturated aqueous uric acid solution at ambient conditions on carbon tape. The crystalline-like uric acid particles appear to be elongated, and the morphology of supermicron uric acid particles was similar to that of anhydrous uric acid reported in a previous work.[21] Crystalline uric acid particles have been extensively studied, and uric acid crystals have been observed to grow epitaxially, resulting in the formation of larger units in the size range of a few microns to a few millimeters.[22] It should be noted that an independent SAED analysis was not conducted on crystalline uric acid particles here.

We use TEM analysis for the nanoparticles, and the results are shown in Figures 3−5. Figure 3 shows the TEM image of uric acid particles generated from the drying of aqueous uric acid solutions on a lacey carbon copper TEM grid. Figure 3a shows a uric acid particle at a magnification of 50k and 200 kV. The circumference of the particle shows the growth of pointed

https://doi.org/10.1021/acsomega.2c01213
ACS Omega 2022, 7, 24202−24207

crystalline structures that could lead to more defined crystalline phase formation. Figure 3b,c shows uric acid particles at a magnification of 100k and 150k and 200k, respectively. The magnified images confirm the formation of small zones of organized atoms, indicative of the formation of a crystalline phase, here on termed as pre-crystallization. Pre-crystallization is different from the layered crystalline structures observed in SEM images (Figure 2). The SAED pattern in Figure 3c shows that the particle is amorphous, and there likely is a weak long-range order in the arrangement of atoms.

The TEM images of uric acid aerosols at two different drying rates (−5 mm Hg and −20 mm Hg) were also taken. Images in Figures 4 and 5 were obtained at a magnification varying from 15k to 40k at 200 kV. Figure 4 shows a selection of nanoparticles dried at the highest drying rate with a vacuum pressure of −20 mm Hg. Particles rapidly dried at −20 mm Hg are composed of smaller subunits. The individual units are easily distinguished and are less than 100 nm (Figure 4). Particle units <100 nm have an elongated shape, while agglomerates appear to be more spherical (Figure 4).

Figure 5 shows uric acid aerosol particles in the size range of 100−200 nm dried more slowly at a drying vacuum pressure of −5 mm Hg. Images in Figure 5 again show that particles at larger sizes are more spherical than particles at smaller sizes. Figure 5 also shows that the individual units forming the particle are smaller and more densely packed. The formation of dry particles is driven by the mobility of the solute and the solvent during evaporation. For low-solubility and high-solute mass compounds, it has been observed that multiple nucleation sites can be formed. Depending on the number of these nucleation sites, the particle can be spheroidal and hollow if a large number of nucleation sites are formed, whereas a low number of nucleation sites can cause particles to be non-spherical.[23]

The diffraction pattern of droplet-dried aerosol particles suggests that the nanoparticles produced were amorphous; HRTEM images show a lack of long-range order of atoms in the aerosol particles (Figure S3). Thus, SEM and TEM images indicate noticeable differences in particle morphology formed by different drying rates (Figures 2−5).

It is difficult to quantify complex morphological changes over a particle size distribution using TEM images. Thus, the AAC-SMPS experimental setup (Figure 1) measured the physical properties (size and shape) of in situ uric acid aerosol. Figure 6 shows the effect of drying rate on the shape factor, χ-value. Figure 6 shows a decrease in χ with increasing aerodynamic diameters, d_{ae}. As uric acid particles become larger, the shape factor approaches that of a spherical particle.

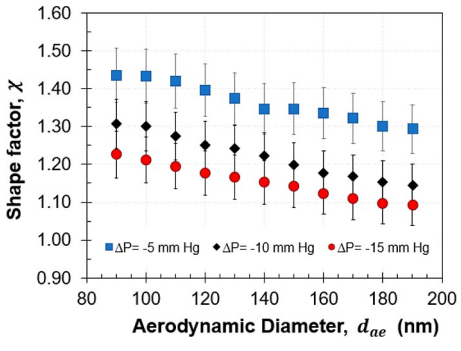

Figure 6. Shape factor vs aerodynamic diameter for uric acid particles.

Furthermore, particles dried rapidly tend to form more spherical particles below 200 nm (Figures 4 and 6). The shape factor values have a known dependence with particle size. For example, the tendency to form more spherical particles at larger sizes was also observed for NaCl particles (w/cuboidal crystalline micron structures) by Wang et al. 2010. The shape factor value for uric acid particles approaches 1.4 for slowly dried particles (at −5 mm Hg), and the value decreases for larger particle sizes (∼200 nm). The shape factor value for smaller particle sizes for fast drying was ∼1.23 and decreases to a value of 1.02 as the particle size increases. Slowly dried particles tend to have higher shape factor values because the morphology of drying particles is a competitive process between the diffusion of solute molecules (uric acid) in the aqueous phase and the diffusion of solvent molecules (water) from the receding surface of the droplet. Particle morphology is hence governed by the relative mobility of two species; an accelerated drying of droplets does not provide enough time for solute molecules to form well-defined structures and can generate voids (Figure 4, Gregson et al. 2019). Uric acid having low solubility and high molecular mass leads to multiple nuclei formation;[26] however, if sufficient time is provided, growing nuclei can fuse together to form compact structures. It is also important to note that with the evaporation of the solute phase, the viscosity of the droplet varies continuously, making the mobility of solute particles even more difficult. The change in drying rate affects the viscosity of the drying droplet; this also impacts the ability of the new phase to nucleate.[25] The shape factor values for uric acid nanonuclei vary in the range of 1.1−1.45 at different drying rates and sizes, suggesting that the particle is non-spherical. For comparison purposes, sodium chloride particles are cubic and have a shape factor value that varies in the range of 1.08−1.24 depending on the drying rate.[24]

4. CONCLUSIONS AND IMPLICATIONS

In summary, evaporation rates alter the morphology (size, shape, and phase) of droplet dried uric acid particles. Faster evaporation tends to form spherical aerosol with smaller particle shape factors, and slower evaporation generates elongated aerosols with higher shape factor values (1.2−1.4). The kidney stone formation in the body is a complex process,[27] and in vivo conditions are difficult to replicate. It has been noted that the proposed model to study uric acid precipitation in pure water is a much simplified model. However, similar binary system models have been used in previous publications to understand the precipitation process.

Previous research has shown that the solution phase has a significant impact on the crystalline structure and solubility of uric acid. In vitro interactions of cations,[28] dyes,[21,29,30] and binding chemicals[31] affect uric acid crystallization in terms of structure and formation rate. However, none of the previous studies have shown the possibility of amorphous uric acid particle formation at submicron sizes. For uric acid, we observed that the crystallization process was slow compared to the time scale of droplet drying; hence, crystalline uric acid particles did not form at the nanoscale. Specifically, uric acid nanonuclei formed in concentrated zones are more likely to be amorphous, irregular-shaped, and non-spherical particles. The shape and consistency of nanonuclei are vastly different from that of the micron-sized particles formed by slow-drying a saturated solution of uric acid on a surface, and the rate of

https://doi.org/10.1021/acsomega.2c01213
ACS Omega 2022, 7, 24202−24207

drying at the macro- and microscale produces much different particles.

Previous work has modeled particle formation from droplet drying with transport and thermodynamic equations.[32−36] However, predicting the morphology of the precipitate has been difficult and requires knowledge of the localized solute concentrations and water activity. Local microscale changes in the solute concentration affect the solution surface tension and contribute to capillary flows in the solution phase (a.k.a., the Marangoni effect; Kuznetsov et al. 2019; Gregson et al. 2019). Thus, the solute morphology is governed by the relative diffusional velocity of the solute and solvent, hence viscosity of the system.[37,38] Additionally, modifying the water activity of an aqueous solution can result in an amorphous phase over a crystalline phase precipitate if the solvent evaporates more rapidly than crystal formation occurs.[25,39,40]

The pre-crystallization phase observed in uric acid nanonuclei is consistent with what we currently know about the early stages of crystal formation for organic compounds. The crystallization of organic salts can be preceded by gel-like structures formed from exposure of the amorphous phase to varying droplet water activity conditions.[39,40] The proclivity of the pre-crystallization phase to organize and crystallize depends on the phase structure. Shahar et al. 2016 showed that the structure of pre-crystallization in aromatic organics is governed by the molecular structure and hydrophobicity of the crystallizing species. Consequently, one can tailor the pre-crystallization phase by tuning the hydrophobicity at various stages of crystallization. It is also important to note that the work here explores the formation of homogeneous uric acid particles from the solution phase. On the contrary, kidney stones in the body are formed from a mixture of organic and inorganic compounds; the presence of seed materials also plays a significant role toward crystallization of organic compounds.[41] Stone formation in the body is not homogeneous, and factors such as the presence of additional salts, pH, and biological material have significant implications on the stone formation process that is much more complex that simplified the droplet drying model.

The kidney stone particle phase will affect the natural and medical chemodissolution processes. Amorphous organics are known to undergo slow hygroscopic growth and deliquescence compared to crystalline particles. Similarly, other surface properties are closely tied with the phase-ordered structures. Amorphous aerosols exhibit gradual deliquescence in the range of 40−80% water activity unlike crystalline aerosols that tend to have a sharp deliquescence point.[39] Thus, both phase and morphology are important toward understanding the interactions of the particle in the solution phase and for corrections toward the water uptake behavior studies of these particles.[40,42] During the initial stages of uric acid precipitation, amorphous phase nanonuclei can form that maybe easier to dissolve over the crystalline deposits that take much longer to form.

At this stage, no in vivo phase studies have confirmed the formation of amorphous particles at the initial stages of stone formation. Our work shows that the possibility of formation of amorphous nano-sized uric acid particles cannot be ignored. Once formed, these amorphous nanoparticles can result in micron-sized crystalline particle formation. The rate of formation governs the phase and morphology of particles at the nanoscale, which affects the growth rate. Previous research shows that uric acid particles with pointed edges and higher kink density grow faster than relatively smooth particles,[8] suggesting that the growth rates are dependent on the morphology of particles. Our experimental findings suggest that the kinetics of precipitation affects the phase, size, and shape of the uric acid particles. Furthermore, the phase of organic species will have a significant effect on subsequent mechanical, dissolution, and water uptake particle behaviors. Our understanding of kidney stone formation must thus be reconsidered based on the new information presented here, and these findings are a step forward in understanding the fundamental particle properties for kidney stone elimination and treatment.

■ ASSOCIATED CONTENT

Supporting Information

The Supporting Information is available free of charge at https://pubs.acs.org/doi/10.1021/acsomega.2c01213.

Exemplary droplet size distribution; ultrafine dry particle size distribution; HRTEM and SAED images of droplet-dried uric acid particles; pressure and RH conditions for different drying rates; and equations for shape factor calculation and error propagation (PDF)

■ AUTHOR INFORMATION

Corresponding Author

Akua Asa-Awuku − *Department of Chemical and Biomolecular Engineering and Department of Chemistry and Biochemistry, University of Maryland, College Park, Maryland 20742, United States;* orcid.org/0000-0002-0354-8368; Email: asaawuku@umd.edu

Author

Dewansh Rastogi − *Department of Chemical and Biomolecular Engineering, University of Maryland, College Park, Maryland 20742, United States;* orcid.org/0000-0002-5416-0048

Complete contact information is available at: https://pubs.acs.org/10.1021/acsomega.2c01213

Author Contributions

D.R. collected the data and analyzed all data sets. Both authors contributed to the development of the study and writing of the manuscript. All authors have given approval to the final version of the manuscript.

Funding

This research work was funded by the National Science Foundation (NSF 1708337 and 2003927).

Notes

The authors declare no competing financial interest.

■ ACKNOWLEDGMENTS

The authors acknowledge the support from the Chemical and Biomolecular Engineering Department at the University of Maryland College Park and the National Science Foundation.

■ REFERENCES

(1) Scales, C. D.; Smith, A. C.; Hanley, J. M.; Saigal, C. S. Prevalence of Kidney Stones in the United States. *Eur. Urol.* **2012**, *62*, 160−165.

(2) Stamatelou, K. K.; Francis, M. E.; Jones, C. A.; Nyberg, L. M.; Curhan, G. C. Time Trends in Reported Prevalence of Kidney Stones in the United States: 1976-1994. *Kidney Int.* **2003**, *63*, 1817−1823.

(3) Ratkalkar, V.; Kleinman, J. Mechanisms of Stone Formation. *Clin. Rev. Bone Miner. Metabol.* **2012**, *9*, 187−197.

(4) Espinosa-Ortiz, E. J.; Eisner, B. H.; Lange, D.; Gerlach, R. Current Insights into the Mechanisms and Management of Infection Stones. *Nat. Rev. Urol.* **2019**, *16*, 35−53.
(5) Sharma, S. K.; Indudhara, R. Chemodissolution of Urinary Uric Acid Stones by Alkali Therapy. *Urol. Int.* **1992**, *48*, 81−86.
(6) Sakhaee, K.; Nicar, M.; Hill, K.; Pak, C. Y. C.; Sakhaee, K. Contrasting Effects of Potassium Citrate and Sodium Citrate Therapies on Urinary Chemistries and Crystallization of Stone-Forming Salts. *Kidney Int.* **1983**, *24*, 348−352.
(7) Kalkura, S. N.; Vaidyan, V. K.; Kanakavel, M.; Ramasamy, P. Crystallization of Uric Acid. *J. Cryst. Growth* **1993**, *132*, 617−620.
(8) Sours, R. E.; Zellelow, A. Z.; Swift, J. A. An in Situ Atomic Force Microscopy Study of Uric Acid Crystal Growth. *J. Phys. Chem. B* **2005**, *109*, 9989−9995.
(9) Presores, J. B.; Swift, J. A. Adhesion Properties of Uric Acid Crystal Surfaces. *Langmuir* **2012**, *28*, 7401−7406.
(10) Liu, F.; Hooks, D. E.; Li, N.; Mara, N. A.; Swift, J. A. Mechanical Properties of Anhydrous and Hydrated Uric Acid Crystals. *Chem. Mater.* **2018**, *30*, 3798−3805.
(11) Lin, R.; Woo, M. W.; Fu, N.; Selomulya, C.; Chen, X. D. In Situ Observation of Taurine Crystallization via Single Droplet Drying. *Dry. Technol.* **2013**, *31*, 1553−1561.
(12) He, G.; Bhamidi, V.; Tan, R. B. H.; Zukoski, C. F.; Zukoski, C. F. Determination of Critical Supersaturation from Microdroplet Evaporation Experiments. *Cryst. Growth Des.* **2006**, *6*, 1175−1180.
(13) Walton, D. E.; Mumford, C. J. Spray Dried Products-Characterization of Particle Morphology. *Chem. Eng. Res. Des.* **1999**, *77*, 21−38.
(14) Walton, D. E. The Morphology of Spray-Dried Particles a Qualitative View. *Dry. Technol.* **2000**, *18*, 1943−1986.
(15) Vehring, R.; Foss, W. R.; Lechuga-Ballesteros, D. Particle Formation in Spray Drying. *J. Aerosol Sci.* **2007**, *38*, 728−746.
(16) Tavakoli, F.; Olfert, J. S. An Instrument for the Classification of Aerosols by Particle Relaxation Time: Theoretical Models of the Aerodynamic Aerosol Classifier. *Aerosol Sci. Technol.* **2013**, *47*, 916−926.
(17) Johnson, T. J.; Irwin, M.; Symonds, J. P. R.; Olfert, J. S.; Boies, A. M. Measuring Aerosol Size Distributions with the Aerodynamic Aerosol Classifier. *Aerosol Sci. Technol.* **2018**, *52*, 655−665.
(18) Yao, Q.; Asa-Awuku, A.; Zangmeister, C. D.; Radney, J. G. Comparison of Three Essential Sub-Micrometer Aerosol Measurements: Mass, Size and Shape. *Aerosol Sci. Technol.* **2020**, *54*, 1197−1209.
(19) Sioutas, C.; Abt, E.; Wolfson, J. M.; Koutrakis, P. Evaluation of the Measurement Performance of the Scanning Mobility Particle Sizer and Aerodynamic Particle Sizer. *Aerosol Sci. Technol.* **1999**, *30*, 84−92.
(20) DeCarlo, P.; Slowik, J.; Worsnop, D.; Davidovits, P.; Jimenez, J. Particle Morphology and Density Characterization by Combined Mobility and Aerodynamic Diameter Measurements. Part 1: Theory. *Aerosol Sci. Technol.* **2004**, *38*, 1185−1205.
(21) Fink, D. A.; Sours, R. E.; Swift, J. A. Modulated Uric Acid Crystal Growth in the Presence of Acridine Dyes. *Chem. Mater.* **2003**, *15*, 2718−2723.
(22) Frincu, M. C.; Fogarty, C. E.; Swift, J. A. Epitaxial Relationships between Uric Acid Crystals and Mineral Surfaces: A Factor in Urinary Stone Formation. *Langmuir* **2004**, *20*, 6524−6529.
(23) Leong, K. H. Morphological Control of Particles Generated from the Evaporation of Solution Droplets: Theoretical Considerations. *J. Aerosol Sci.* **1987**, *18*, 511−524.
(24) Wang, Z.; King, S. M.; Freney, E.; Rosenoern, T.; Smith, M. L.; Chen, Q.; Kuwata, M.; Lewis, E. R.; Pöschl, U.; Wang, W.; Buseck, P. R.; Martin, S. T. The Dynamic Shape Factor of Sodium Chloride Nanoparticles as Regulated by Drying Rate. *Aerosol Sci. Technol.* **2010**, *44*, 939−953.
(25) Gregson, F. K. A.; Robinson, J. F.; Miles, R. E. H.; Royall, C. P.; Reid, J. P. Drying Kinetics of Salt Solution Droplets: Water Evaporation Rates and Crystallization. *J. Phys. Chem. B* **2019**, *123*, 266−276.
(26) Leong, K. H. Morphological Control of Particles Generated from the Evaporation of Solution Droplets: Theoritical Considerations. *J. Aerosol Sci.* **1986**, *18*, 511−524.
(27) Dawson, C. H.; Tomson, C. R. Kidney Stone Disease: Pathophysiology, Investigation and Medical Treatment. *Clin. Med.* **2012**, *12*, 467−471.
(28) Mcnabb, R. A.; Mcnabb, F. M. A. Physiological Chemistry of Uric Acid : Solubility, Colloid and Ion Binding Properties. *Comp. Biochem. Physiol.* **1980**, *67*, 27−34.
(29) Sours, R. E.; Fink, D. A.; Swift, J. A. Dyeing Uric Acid Crystals with Methylene Blue. *J. Am. Chem. Soc.* **2002**, *124*, 8630−8636.
(30) Hall, V. M.; Cox, K. A.; Sours, R. E.; Swift, J. A. Urochrome Pigment in Uric Acid Crystals. *Chem. Mater.* **2016**, *28*, 3862−3869.
(31) Hall, V. M.; Thornton, A.; Miehls, E. K.; Bertke, J. A.; Swift, J. A. Uric Acid Crystallization Interrupted with Competing Binding Agents. *Cryst. Growth Des.* **2019**, *19*, 7363−7371.
(32) Mezhericher, M.; Levy, A.; Borde, I. Theoretical Models of Single Droplet Drying Kinetics: A Review. *Dry. Technol.* **2010**, *28*, 278−293.
(33) Gac, J. M.; Gradoń, L. A Distributed Parameter Model for the Spray Drying of Multicomponent Droplets with a Crust Formation. *Adv. Powder Technol.* **2013**, *24*, 324−330.
(34) Seydel, P.; Blömer, J.; Bertling, J. Modeling Particle Formation at Spray Drying Using Population Balances. *Dry. Technol.* **2006**, *24*, 137−146.
(35) Maurice, U.; Mezhericher, M.; Levy, A.; Borde, I. Drying of Droplet Containing Insoluble Nanoscale Particles: Numerical Simulations and Parametric Study. *Dry. Technol.* **2013**, *31*, 1790−1807.
(36) Maurice, U.; Mezhericher, M.; Levy, A.; Borde, I. Drying of Droplets Containing Insoluble Nanoscale Particles: Second Drying Stage. *Dry. Technol.* **2015**, *33*, 1837−1848.
(37) Kuznetsov, G. V.; Misyura, S. Y.; Volkov, R. S.; Morozov, V. S. Marangoni Flow and Free Convection during Crystallization of a Salt Solution Droplet. *Colloids Surf. A Physicochem. Eng. Asp.* **2019**, *572*, 37−46.
(38) Gregson, F. K. A.; Robinson, J. F.; Miles, R. E. H.; Royall, C. P.; Reid, J. P. Drying and Crystallization of Evaporating Sodium Nitrate Aerosol Droplets. *J. Phys. Chem. B* **2020**, *124*, 6024−6036.
(39) Mikhailov, E.; Vlasenko, S.; Martin, S. T.; Koop, T.; Pöschl, U. Amorphous and Crystalline Aerosol Particles Interacting with Water Vapor: Conceptual Framework and Experimental Evidence for Restructuring, Phase Transitions and Kinetic Limitations. *Atmos. Chem. Phys.* **2009**, *9*, 9491−9522.
(40) Saukko, E.; Kuuluvainen, H.; Virtanen, A. A Method to Resolve the Phase State of Aerosol Particles. *Atmos. Meas. Tech.* **2012**, *5*, 259−265.
(41) Shahar, C.; Dutta, S.; Weissman, H.; Shimon, L. J. W.; Ott, H.; Rybtchinski, B. Precrystalline Aggregates Enable Control over Organic Crystallization in Solution. *Angew. Chem.* **2016**, *128*, 187−190.
(42) Altaf, M. B.; Dutcher, D. D.; Raymond, T. M.; Freedman, M. A. Effect of Particle Morphology on Cloud Condensation Nuclei Activity. *ACS Earth Space Chem.* **2018**, *2*, 634−639.

https://doi.org/10.1021/acsomega.2c01213
ACS Omega 2022, 7, 24202−24207